Bull. Chem. Soc. Ethiop. **2026**, 40(12), 2701-2716.
DOI: https://dx.doi.org/10.4314/bcse.v40i12.14

ISSN 1011-3924
Printed in Ethiopia
Online ISSN 1726-801X
© 2026 Chemical Society of Ethiopia and The Authors

GREEN SYNTHESIS OF rGO/ZnO/Fe_2O_3 USING *CAULERPA PELTATA* EXTRACT FOR ENHANCED MALACHITE GREEN REMOVAL

Said Ali Akbar[1*], Muhammad Hasan[2], Cut Nuzlia[1]

[1]Department of Aquaculture, Faculty of Marine and Fisheries, Universitas Syiah Kuala, Banda Aceh, 23111, Indonesia
[2]Department of Chemistry Education, Faculty of Teacher Training and Education, Universitas Syiah Kuala, Banda Aceh 23111, Aceh, Indonesia

(Received November 17, 2025; Revised March 28, 2026; Accepted August 17, 2026)

ABSTRACT. This study reports the green synthesis of rGO/ZnO/Fe_2O_3 nanocomposites using Caulerpa peltata extract as a natural reducing and stabilizing agent for enhanced malachite green (MG) removal from aqueous solutions. Structural characterization confirmed successful composite formation, where XRD analysis revealed the coexistence of crystalline ZnO and Fe_2O_3 phases integrated within the rGO matrix, while FTIR, Raman, and thermogravimetric analyses indicated successful reduction, increased defect density, and improved thermal stability. Raman analysis showed an increase in I_D/I_G ratio from 1.197 to 1.283 after composite formation, suggesting additional active defect sites. Adsorption studies demonstrated superior performance of rGO/ZnO/Fe_2O_3 with a maximum adsorption capacity of 305.212 mg g^{-1} compared to 190.582 mg g^{-1} for rGO. The adsorption process followed pseudo-second-order kinetics and showed spontaneous, exothermic behavior. Furthermore, the composite maintained removal efficiencies above 94% after ten adsorption–desorption cycles, indicating excellent operational stability and reusability for sustainable wastewater treatment applications.

KEY WORDS: Reduced graphene oxide, Green synthesis, *Caulerpa peltate*, Malachite green adsorption, rGO/ZnO/Fe_2O_3 nanocomposite

INTRODUCTION

Water pollution caused by industrial effluents remains one of the most pressing environmental challenges worldwide, particularly in regions with intensive textile production and aquaculture activities [1]. Among various contaminants, synthetic dyes such as malachite green are of significant concern due to their widespread use as coloring agents and antifungal treatments. Although effective in industrial and aquaculture applications, malachite green is highly toxic, mutagenic, and potentially carcinogenic, posing serious risks to aquatic ecosystems and human health. Its chemical stability and resistance to biodegradation further complicate its removal from wastewater, allowing it to persist in natural water bodies for extended periods [2]. Conventional treatment methods, including coagulation and flocculation processes, advanced oxidation techniques, membrane filtration systems, and biological treatments, have been widely applied. However, these approaches often involve high operational costs, complex infrastructure, production of secondary sludge, and limited efficiency at low dye concentrations. In this context, adsorption has emerged as a promising alternative because of its operational simplicity, economic feasibility, flexibility, and high removal efficiency across a broad concentration range [3]. The effectiveness of adsorption systems strongly depends on the physicochemical properties of the adsorbent material [4,5]. Therefore, there is an urgent need to develop advanced adsorbents that exhibit high adsorption capacity, structural stability, reusability, and environmental compatibility [6,7]. The development of efficient materials through sustainable synthesis strategies is essential to ensure that wastewater treatment technologies remain both effective and environmentally responsible.

*Corresponding authors. E-mail: saidaliakbar@usk.ac.id
This work is licensed under the Creative Commons Attribution 4.0 International License

Graphene-based materials have attracted considerable attention as adsorbents due to their unique structural and physicochemical properties. Graphene oxide (GO) possesses abundant oxygen-containing functional groups such as hydroxyl, epoxy, and carboxyl groups, which enhance hydrophilicity and provide active binding sites for dye molecules [8]. After reduction, reduced graphene oxide (rGO) partially restores the sp^2 carbon network, increasing electrical conductivity and strengthening π–π interactions with aromatic pollutants such as malachite green [9]. Owing to its high specific surface area, theoretically reaching up to 2630 $m^2\ g^{-1}$ for graphene-based structures, rGO has demonstrated adsorption capacities exceeding 200 mg g^{-1} for various organic dyes in previous studies. However, the practical application of single-component rGO remains limited due to sheet aggregation driven by van der Waals interactions, reduced dispersion stability in aqueous media, and challenges in post-treatment separation and recovery [10]. To overcome these limitations, hybridization with metal oxides such as ZnO and Fe_2O_3 has been explored to enhance structural stability, increase active surface sites, and introduce magnetic properties that facilitate separation. ZnO contributes additional adsorption and potential photocatalytic activity, while Fe_2O_3 enables magnetic recovery and improves structural integrity [11]. Conventional chemical reduction methods for producing rGO often involve hazardous reducing agents such as hydrazine, which pose environmental and safety concerns [12]. In this context, biomass extracts containing polyphenols and other bioactive compounds offer a greener alternative for reducing GO [13, 14, 15]. Marine algae such as *Caulerpa peltata* contain natural antioxidants capable of donating electrons to facilitate reduction. Despite growing interest in green synthesis approaches, studies on ternary rGO/ZnO/Fe_2O_3 composites prepared using algae-based extracts remain limited, particularly those providing detailed mechanistic correlations between structural characteristics and adsorption performance.

This study presents the eco-friendly synthesis of a rGO/ZnO/Fe_2O_3 ternary composite using *Caulerpa peltata* extract as a natural reducing agent and stabilizing medium [5,16]. The approach integrates green chemistry principles with advanced material design to produce a multifunctional adsorbent for malachite green removal. These analyses enable detailed assessment of structural evolution from GO to rGO and subsequent integration with ZnO and Fe_2O_3 phases. The adsorption performance of the composite was comprehensively evaluated through equilibrium isotherm modeling, kinetic studies, thermodynamic analysis, and multi-cycle reusability testing to assess stability and operational durability. Particular attention was given to correlating structural parameters, such as restoration of sp^2 domains and modification of oxygen-containing functional groups, with adsorption capacity, interaction strength, and spontaneity of the process [17,18]. By combining a green synthesis route, a ternary metal oxide–graphene composite system, and an integrated mechanistic evaluation, this work provides a deeper understanding of structure–performance relationships in dye adsorption systems. The findings contribute to the development of sustainable, high-performance adsorbent materials and expand current knowledge on environmentally benign fabrication strategies for advanced wastewater treatment applications.

MATERIALS AND METHODS

Materials

The chemicals used in this study were graphite powder (200 mesh), potassium permanganate ($KMnO_4$), sulfuric acid (H_2SO_4, 97–98%), sodium nitrate ($NaNO_3$), hydrogen peroxide (H_2O_2, 30%), sodium hydroxide (NaOH), zinc nitrate hexahydrate ($Zn(NO_3)_2{\cdot}6H_2O$), ferric nitrate nonahydrate ($Fe(NO_3)_3{\cdot}9H_2O$), deionized water, ethanol, and Whatman No. 1 filter paper. *Caulerpa peltata* was used as the macroalgal biomass for preparation of the aqueous extract employed as a natural reducing and stabilizing agent during the synthesis of rGO and the rGO/ZnO/Fe_2O_3 ternary composite.

Preparation of graphene oxide (GO)

Graphene oxide was synthesized using a modified Hummers method [3]. To control the temperature, 1 g of graphite powder, 23 mL of concentrated sulfuric acid (H_2SO_4), and 0.5 g of sodium nitrate ($NaNO_3$) were mixed and placed in an ice bath. After thorough stirring, 3 grams of potassium permanganate ($KMnO_4$) were gradually added while keeping the temperature below 10°C to prevent overheating. The mixture was stirred at room temperature for twelve hours to continue the oxidation process. Following oxidation, the solution was diluted with 100 mL of deionized water. Then, 30 mL of 3% hydrogen peroxide (H_2O_2) was slowly added to neutralize the remaining potassium permanganate. The appearance of a bright yellow solution confirmed the successful formation of graphene oxide. The suspension was then centrifuged, and the supernatant was discarded. The solid graphene oxide was thoroughly washed several times with deionized water to remove impurities and dried in an oven at 60°C to obtain the final graphene oxide product.

Preparation of plant extracts

Fresh *Caulerpa peltata* was collected and thoroughly washed using deionized water to remove attached debris, sand, and impurities [3, 4]. The cleaned biomass was air-dried at room temperature (27-30 °C) for 48 h to reduce moisture content before being ground into fine powder using a mortar and pestle. Subsequently, 10 g of dried *Caulerpa peltata* powder was mixed with 100 mL of deionized water and heated at 80 °C for 60 min under continuous magnetic stirring at 500 rpm to extract bioactive compounds. After extraction, the suspension was cooled to room temperature and filtered using Whatman No. 1 filter paper to separate solid residues from the liquid extract. The obtained filtrate was collected and stored at 4 °C prior to use. This extract was subsequently utilized as a natural reducing and stabilizing agent during the reduction of graphene oxide and composite synthesis processes.

Preparation of reduced graphene oxide (rGO)

The reduction of graphene oxide (GO) to reduced graphene oxide (rGO) was performed using *Caulerpa peltata* extract as a natural reducing agent [5]. Initially, 100 mg of GO powder was dispersed in 100 mL of deionized water to obtain a 1 mg mL^{-1} suspension, followed by ultrasonication for 30 min to achieve homogeneous dispersion. Subsequently, 50 mL of freshly prepared *Caulerpa peltata* extract (prepared from 10 g dried biomass in 100 mL deionized water) was slowly added to the GO suspension under continuous magnetic stirring. The reaction mixture was heated at 90 °C for 2 h under constant stirring at 500 rpm without additional pH adjustment to facilitate the reduction process. During the reaction, the suspension gradually changed from brown to black, indicating the conversion of GO into rGO. After completion, the suspension was cooled to room temperature and centrifuged at 4000 rpm for 15 min. The collected precipitate was washed three times using deionized water to remove residual impurities and unreacted compounds. Finally, the purified rGO was dried in a vacuum oven at 60 °C for 24 h and stored in a desiccator prior to characterization and adsorption experiments.

Preparation of rGO/ZnO/Fe_2O_3 composite

The rGO/ZnO/Fe_2O_3 ternary composite was synthesized using a green-assisted hydrothermal method with *Caulerpa peltata* extract as a natural reducing and stabilizing agent. Initially, 100 mg of the previously prepared rGO was dispersed in 50 mL of deionized water and ultrasonicated for 30 min to obtain a homogeneous suspension. Subsequently, 0.5 g of zinc nitrate hexahydrate ($Zn(NO_3)_2 \cdot 6H_2O$) and 0.5 g of ferric nitrate nonahydrate ($Fe(NO_3)_3 \cdot 9H_2O$) were added to the rGO suspension under continuous magnetic stirring. Based on the stoichiometric conversion of the

metal nitrate precursors to their corresponding oxides, these amounts theoretically correspond to approximately 0.137 g ZnO and 0.099 g Fe_2O_3, giving a targeted ZnO:rGO_2O_3 mass ratio of approximately 1.37:1.00:0.99 (w/w/w). The mixture was continuously stirred to promote homogeneous distribution and interaction of Zn^{2+} and Fe^{3+} species with the rGO sheets. *Caulerpa peltata* extract was then introduced into the reaction mixture as a green reducing and stabilizing medium. The resulting suspension was transferred into a Teflon-lined stainless-steel autoclave and subjected to hydrothermal treatment at 180 °C for 12 h to promote the formation and deposition of ZnO and Fe_2O_3 nanoparticles onto the rGO surface. After completion of the reaction, the autoclave was allowed to cool naturally to room temperature. The resulting rGO/ZnO/Fe_2O_3 composite was collected by centrifugation and washed several times with deionized water and ethanol to remove residual and unreacted species. Finally, the purified composite was dried in a vacuum oven at 60 °C for 12 h and stored in a desiccator prior to physicochemical characterization and adsorption experiments.

Characterizations

Structural and morphological characterizations were performed to analyze the physicochemical properties of the synthesized materials. X-ray diffraction (XRD) was used to identify crystalline phases and structural characteristics. The measurements were conducted using a PANalytical X'Pert Pro diffractometer at CAE, Montreal, Canada. Surface morphology and particle distribution were examined using scanning electron microscopy (SEM) with a Tescan Mira 3 instrument to obtain detailed images at micro- and nanoscale levels. Fourier transform infrared spectroscopy (FTIR) was employed to identify functional groups and chemical bonding in the synthesized materials. FTIR spectra were recorded using a Shimadzu FT-IR-8400S spectrophotometer (Japan) in the range of 400-4000 cm^{-1} with a resolution of 4 cm^{-1} using the KBr pellet technique. Raman spectroscopy was performed using a Horiba Raman spectrometer equipped with a 532 nm excitation laser to evaluate structural defects, graphitic ordering, and defect density of the synthesized materials. Ultraviolet–visible (UV–Vis) spectroscopy was used to determine the optical absorption characteristics of the samples using a Shimadzu 1601 UV–Vis spectrophotometer (Tokyo, Japan). Thermogravimetric analysis (TGA) was carried out using a TG 209 F3 Tarsus instrument (NETZSCH Thermal Analysis, Germany) under a nitrogen atmosphere at a heating rate of 10 °C min^{-1} from room temperature to 500 °C to evaluate the thermal stability of the materials.

Adsorption procedure

The adsorption experiment for malachite green (MG) removal was conducted using the synthesized adsorbent materials. In a typical experiment, 5 mg of adsorbent was added to a glass vial containing 10 mL of malachite green solution with an initial concentration of 1 ppm. The mixture was placed in a temperature-controlled shaker at 25 °C and agitated at 150 rpm to allow the adsorption process to occur. After the predetermined contact time, the suspension was filtered to separate the adsorbent from the solution. The remaining concentration of malachite green in the filtrate was determined using a UV-Vis spectrophotometer at a wavelength of 618 nm, corresponding to the maximum absorbance peak of malachite green. The adsorption performance was evaluated by calculating the removal efficiency based on the difference between the initial and equilibrium dye concentrations.

$$\% \text{ Removal} = \frac{C_0 - C_e}{C_0} \times 100\% \quad (1)$$

The formula to calculate the percentage removal of Malachite Green (or any adsorbate) shown in Equation (1), where C_0 is Initial concentration of Malachite Green (mg/L or ppm), C_e is

Equilibrium (or final) concentration of Malachite Green after adsorption (mg/L or ppm). This formula calculates the percentage of the initial concentration of Malachite Green that has been adsorbed and removed from the solution by the adsorbent.

RESULTS AND DISCUSSION

Physicochemical characterization of rGO/ZnO/Fe_2O_3 nanocomposites

The XRD patterns of Fe_2O_3, ZnO, rGO, and the synthesized rGO/ZnO/Fe_2O_3 composite are presented in Figure 1a. The diffraction pattern of Fe_2O_3 exhibits characteristic peaks at 2θ values around 24.1°, 33.2°, 35.6°, 40.9°, 49.5°, 54.1°, 57.5°, 62.4°, and 64.0°, corresponding to the crystallographic planes of (012), (104), (110), (113), (024), (116), (018), (214), and (300), respectively, confirming the formation of hematite phase [8-10]. ZnO displays distinct diffraction peaks located at approximately 31.8°, 34.4°, 36.2°, 47.5°, 56.6°, 62.8°, 66.3°, 67.9°, 72.6°, and 76.9°, which can be indexed to the hexagonal wurtzite structure corresponding to the planes (100), (002), (101), (102), (110), (103), (200), (112), (004), and (202), respectively [11,19]. The diffraction pattern of rGO shows a broad peak centered at approximately 24-25°, assigned to the (002) reflection, indicating the restoration of graphitic domains after reduction while maintaining a relatively disordered layered structure. The broadening of this peak suggests incomplete restacking and the presence of residual defects and structural disorder within the reduced graphene sheets [20]. Following composite formation, the XRD pattern of rGO/ZnO/Fe_2O_3 retains the characteristic diffraction peaks of both ZnO and Fe_2O_3 without noticeable peak shifting, suggesting that the crystal structures of both metal oxide phases remain preserved during synthesis. The broad rGO diffraction band around 24–25° remains visible but with lower prominence due to overlap with nearby metal oxide reflections. The simultaneous presence of diffraction peaks belonging to rGO, ZnO, and Fe_2O_3 indicates successful incorporation of both oxide phases onto the graphene matrix, while the relatively lower intensity of several Fe_2O_3 reflections compared to ZnO suggests that the oxide phases are dispersed within the composite rather than existing as highly segregated crystalline domains [8-11,19, 20].

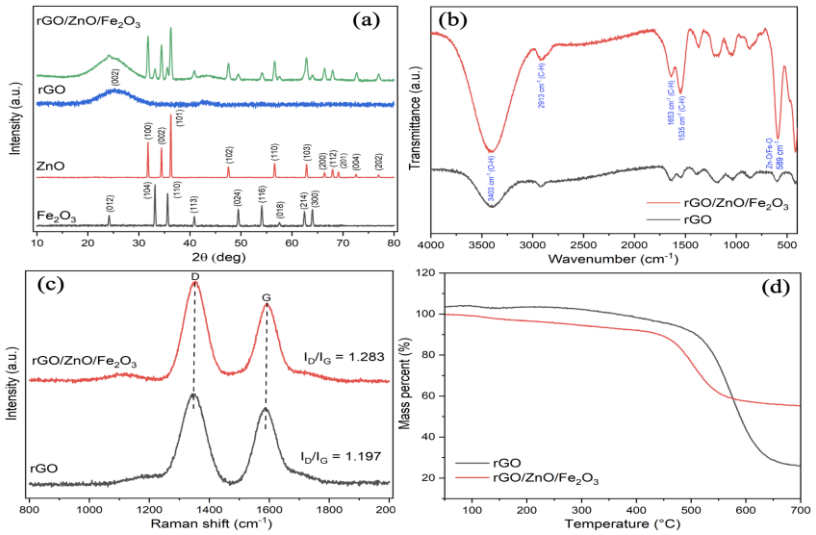

Figure 1. (a) XRD patterns, (b) FTIR spectra, (c) Raman spectra, and (d) thermogravimetric analysis (TGA) of rGO and rGO/ZnO/Fe_2O_3 composites.

The FTIR spectra of rGO and rGO/ZnO/Fe_2O_3 are presented in Figure 1b to evaluate the functional groups and structural modifications after composite formation. The FTIR spectrum of rGO exhibits a broad absorption band centered around 3403 cm^{-1}, corresponding to O–H stretching vibrations associated with residual hydroxyl groups and adsorbed moisture remaining after the reduction process [12, 21]. The relatively weak absorption bands observed in the fingerprint region indicate that most oxygen-containing functionalities have been removed, consistent with the partial restoration of graphitic structures in reduced graphene oxide [22]. Following composite formation, the FTIR spectrum of rGO/ZnO/Fe_2O_3 displays several additional absorption bands, indicating successful incorporation of metal oxide phases and surface interactions between rGO and inorganic components. The broad O–H stretching band remains visible but becomes more intense, suggesting contributions from surface hydroxyl groups associated with metal oxides and biomolecules derived from Caulerpa peltata extract [23]. The absorption band at 2913 cm^{-1} is attributed to C–H stretching vibrations, while the peaks observed at 1653 cm^{-1} and 1535 cm^{-1} correspond to C=C skeletal vibrations and residual carbon-related functional groups within the graphene framework [21, 24]. Most importantly, the appearance of strong absorption bands in the low wavenumber region, particularly around 589 cm^{-1}, can be assigned to Zn–O and Fe–O lattice vibrations, confirming the formation of metal oxide structures within the composite matrix [12, 23]. The increased complexity of absorption features in the fingerprint region further suggests interactions between rGO sheets and metal oxide nanoparticles, which may contribute to changes in surface chemistry and interfacial bonding within the synthesized composite [21, 24].

The Raman spectra and thermogravimetric analysis (TGA) of rGO and rGO/ZnO/Fe_2O_3 are presented in Figures 1c and 1d to evaluate structural disorder and thermal stability after composite formation. The Raman spectra of both samples display two characteristic bands centered at approximately 1350 cm^{-1} (D band) and 1590 cm^{-1} (G band), corresponding to defect-induced vibrations and graphitic sp^2 carbon structures, respectively [12, 21]. The calculated I_D/I_G ratio increases from 1.197 for rGO to 1.283 after incorporation of ZnO and Fe_2O_3, indicating increased structural defects, lattice distortion, and additional disorder generated by the interaction between metal oxide nanoparticles and graphene sheets [22, 23]. The increase in defect density may promote the formation of additional active sites and improve surface interactions, which is advantageous for adsorption applications [24]. Thermal stability analysis further supports successful composite formation. Pure rGO exhibits relatively stable mass retention at lower temperatures followed by substantial weight loss above approximately 500 °C, resulting in a final residual mass of around 25–30%, primarily due to decomposition of carbonaceous structures [21]. In contrast, rGO/ZnO/Fe_2O_3 demonstrates improved thermal stability with a slower degradation profile and significantly higher residual mass (~55%) at 700 °C. The higher residual fraction is attributed to the presence of thermally stable inorganic oxide phases that remain after decomposition of carbon components, while the delayed mass loss behavior suggests that interactions between rGO sheets and metal oxide particles improve resistance toward thermal degradation [12, 23, 24].

Electrochemical analysis

The electrochemical analysis shows significant differences in the performance of rGO and rGO/ZnO/Fe_2O_3, particularly in their impedance, conductivity, and voltammetric behaviors. From the electrochemical impedance spectroscopy (EIS), the Nyquist plots reveal that rGO/ZnO/Fe_2O_3 has a lower solution resistance (R_s) of 89 ohms and a much lower charge transfer resistance (R_{ct}) of 220 ohms compared to rGO, which has R_s of 100 ohms and R_{ct} of 610 ohms (Figure 2c) [10,19]. This reduction in R_{ct} for rGO/ZnO/Fe_2O_3 highlights its improved electron transfer properties, due to the partial removal of oxygen functional groups, leading to enhanced conductivity. The circuit

model, which includes a constant phase element (CPE) in parallel with R_{ct}, capacitance (C), and Warburg impedance (W), supports these findings, as the lower R_{ct} in rGO/ZnO/Fe_2O_3 suggests more efficient charge transfer, making it a better conductor than rGO. This is further corroborated by the conductivity measurements, where rGO/ZnO/Fe_2O_3 exhibits increasing electrical conductivity with temperature, as shown in the rGO/ZnO/Fe_2O_3 Mott's plot and the conductivity vs. temperature graph (Figure 2a and 2b). The linear fitting of rGO/ZnO/Fe_2O_3's Mott's plot, with a high R^2 value of 0.99826, indicates consistent electrical behavior as the temperature increases, supporting the fact that rGO/ZnO/Fe_2O_3 has improved conductivity due to the restoration of sp^2 bonding networks.

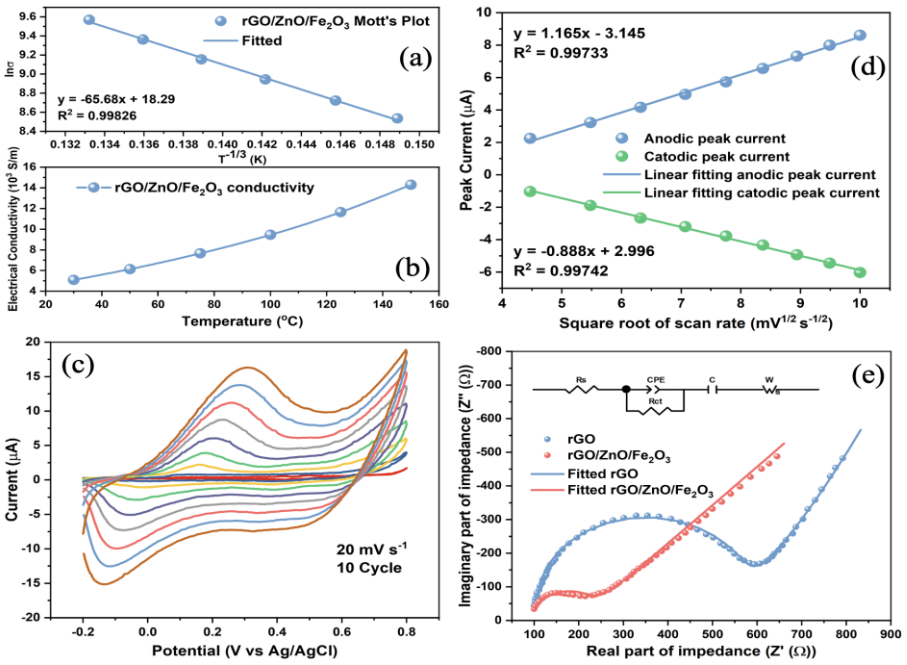

Figure 2. (a) Mott plot for rGO/ZnO/Fe_2O_3, (b) Conductivity of rGO/ZnO/Fe_2O_3, (c) Nyquist plot comparing experimental and fitted impedance data for both rGO and rGO/ZnO/Fe_2O_3, (d) Cyclic voltammetry response of rGO/ZnO/Fe_2O_3 in a 0.1 M KCl solution containing 5 mM $Fe(CN)_6^{3-/4-}$ at a scan rate of 50 mV/s, (e) Relationship between anodic and cathodic peak currents and scan rate for rGO/ZnO/Fe_2O_3.

These results are further supported by the voltammetric study; the cyclic voltammograms of rGO/ZnO/Fe_2O_3 show more prominent redox peaks than those of rGO, suggesting stronger electrochemical activity. The anodic and cathodic peak currents' linear relationship with the scan rate's square root (R^2 = 0.99742 for cathodic peaks and R^2 = 0.99733 for anodic peaks) indicates that the redox reactions on rGO/ZnO/Fe_2O_3 are diffusion-controlled, supporting its superior electrochemical qualities over rGO [10, 19].

Microscopic studies

The SEM images provide important insights into the morphological differences between rGO and the rGO/ZnO/Fe_2O_3 composite. Image (a) shows rGO with a typical wrinkled and layered sheet-

like structure, where thin graphene layers are stacked and partially restacked due to van der Waals interactions. The surface appears relatively compact with overlapping flakes, indicating partial restoration of the sp^2 carbon network after reduction. Although the sheets are more ordered than GO, some aggregation is still evident, which may limit the accessibility of active adsorption sites. In contrast, image (b) reveals noticeable morphological changes after incorporation of ZnO and Fe_2O_3. The rGO/ZnO/Fe_2O_3 composite exhibits a more heterogeneous and textured surface, where metal oxide particles are distributed on and between the graphene sheets [25, 26]. This dispersion prevents excessive restacking of rGO layers, resulting in a more open and structurally integrated architecture. The presence of ZnO and Fe_2O_3 nanoparticles contributes to increased surface roughness and additional active sites, which enhance adsorption interactions. Furthermore, the composite structure appears more structurally interconnected, suggesting improved stability and resistance to sheet aggregation.

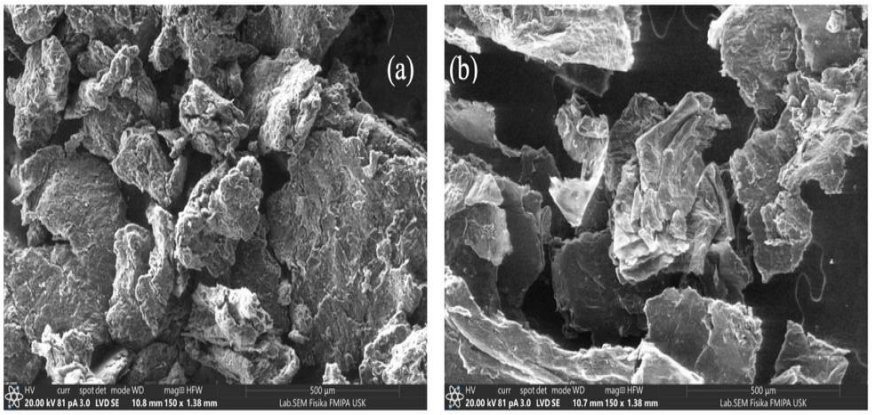

Figure 3. SEM analysis with magnification 150x for (a) rGO and (b) rGO/ZnO/Fe_2O_3

Dye removal study: Effect of pH

The removal of malachite green (MG) by rGO and rGO/ZnO/Fe_2O_3 was evaluated over a wide pH range, and the results demonstrate a strong dependence of adsorption efficiency on solution pH. As shown in Figure 4, rGO/ZnO/Fe_2O_3 consistently exhibits significantly higher removal efficiency than rGO at all investigated pH values [20, 22]. At acidic conditions (pH 3), the removal efficiency of rGO is relatively low, whereas the composite already shows markedly improved performance. As the pH increases, the adsorption efficiency of both materials rises progressively, reaching maximum values at alkaline conditions (around pH 9-10), where rGO/ZnO/Fe_2O_3 achieves removal efficiencies exceeding 90%, while rGO remains substantially lower. This behavior can be explained by surface charge effects and the chemical nature of malachite green, which exists predominantly as a cationic dye in aqueous solution. At low pH, protonation of functional groups on the adsorbent surface reduces electrostatic attraction between the positively charged dye molecules and the adsorbent. With increasing pH, deprotonation of surface hydroxyl and oxygen-containing groups enhances the negative surface charge, strengthening electrostatic interactions. In the composite system, the presence of ZnO and Fe_2O_3 introduces additional active sites and surface hydroxyl groups, further promoting electrostatic attraction and possibly surface complexation. The improved structural dispersion of rGO sheets within the composite also prevents restacking, increasing accessible adsorption sites and explaining the superior performance of rGO/ZnO/Fe_2O_3 across the studied pH range [23, 24].

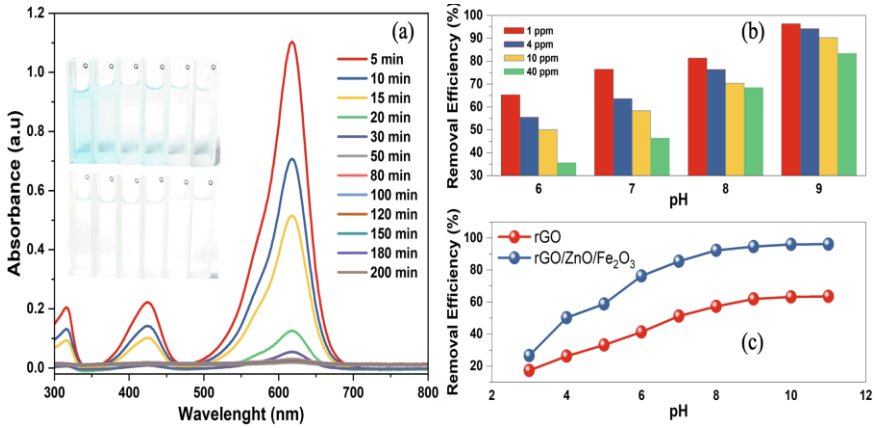

Figure 4. Removal of MG using rGO/ZnO/Fe_2O_3 (a) Change in absorbance with time (b) (c) variation in removal percentage for rGO and rGO/ZnO/Fe_2O_3 by different pH.

The removal efficiency at different initial MG concentrations was further evaluated at pH 9 over a 30-minute contact period, as shown in Figure 4. The rGO/ZnO/Fe_2O_3 composite consistently exhibited higher removal efficiency than rGO across all tested concentrations. At low concentration (1 ppm), the composite achieved removal above 95%, while maintaining relatively high efficiency even at 40 ppm, indicating strong adsorption capability. As expected, the percentage removal decreased with increasing initial dye concentration due to progressive occupation and partial saturation of available active sites. The UV–Vis absorbance spectra show a pronounced decrease in the characteristic MG peak at approximately 620 nm with increasing contact time, particularly within the first 30 minutes, confirming rapid adsorption kinetics [25,27]. The visible color change from intense green to nearly colorless further supports the spectroscopic results. The enhanced performance of rGO/ZnO/Fe_2O_3 can be attributed to improved surface accessibility, additional active sites provided by ZnO and Fe_2O_3, and reduced restacking of graphene layers, which collectively promote stronger electrostatic interactions and π–π stacking with MG molecules.

Effect of temperature and contact time

The removal of malachite green (MG) as a function of contact time and temperature for rGO and rGO/ZnO/Fe_2O_3 shows distinct adsorption behavior, as presented in Figure 5a and 5b. For both materials, the removal efficiency increases rapidly during the initial stage and approaches equilibrium within approximately 50 minutes, reflecting progressive occupation of available adsorption sites. At 25°C, rGO achieves a removal efficiency of about 94-96% after 200 minutes, whereas rGO/ZnO/Fe_2O_3 reaches approximately 72-74% under the same conditions [20, 22, 26, 28]. As the temperature increases to 55°C, the efficiency decreases for both adsorbents, with rGO dropping to around 50% and the composite to approximately 48-50%. The decline in performance at higher temperatures indicates that the adsorption process is exothermic, where increased thermal motion weakens electrostatic attraction and π–π interactions between MG molecules and the adsorbent surface. The presence of ZnO and Fe_2O_3 within the graphene matrix modifies surface characteristics, alters site distribution, and affects thermal response, which is reflected in the different adsorption profiles observed across the tested temperatures [3-5, 29].

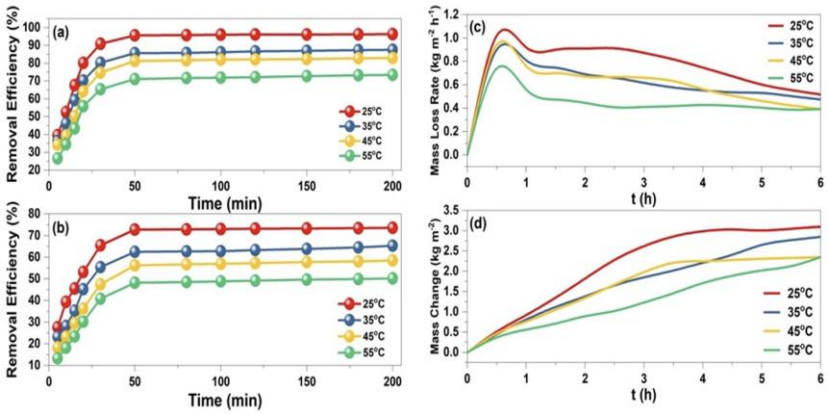

Figure 5. Effect of temperature and contact time on removal of MG using (a) rGO and (b) rGO/ZnO/Fe_2O_3, (c) mass loss curves and (d) and evaporation rate curves for Photothermal properties of rGO/ZnO/Fe_2O_3 after adsorption.

The photothermal behavior of rGO/ZnO/Fe_2O_3 after malachite green (MG) adsorption was examined through mass change and evaporation rate profiles at different temperatures, as shown in Figure 5c and 5d. Over a six-hour period, the cumulative mass change is higher at 25°C, reaching approximately 3.1 units, whereas at 55°C it remains lower at around 2.35 units [20, 22, 23, 30]. The evaporation rate curves display a similar pattern, with an initial peak followed by gradual stabilization. At 25°C, the rate begins at about 1.02 kg m^{-2} h^{-1} within the first 0.5 hours and decreases to approximately 0.52 kg m^{-2} h^{-1} after six hours, while at 55°C it starts near 0.74 kg m^{-2} h^{-1} and stabilizes around 0.39 kg m^{-2} h^{-1}. These temperature-dependent variations reflect differences in surface interaction strength and thermal response of the adsorbed MG molecules. The incorporation of ZnO and Fe_2O_3 within the rGO framework alters heat distribution and interfacial behavior, which is reflected in the distinct mass change and evaporation profiles observed under varying thermal conditions.

Isothermal Adsorption Analysis

Several isotherm models were applied to evaluate the adsorption behavior of malachite green on rGO and rGO/ZnO/Fe_2O_3, as summarized in Table 1. According to the Langmuir model, rGO/ZnO/Fe_2O_3 exhibits a higher maximum adsorption capacity (Qmax) of 305.212 mg g^{-1} compared to 190.582 mg g^{-1} for rGO, indicating enhanced monolayer adsorption on the composite surface. The Langmuir correlation coefficients are 0.998 for rGO/ZnO/Fe_2O_3 and 0.985 for rGO, suggesting that the adsorption process is well described by the Langmuir assumption of uniform active sites, particularly for the composite [3, 4]. The Freundlich model further reflects stronger adsorption intensity for rGO/ZnO/Fe_2O_3, with higher Kf (199.523) and n (2.643) values compared to rGO (Kf = 61.450; n = 1.952), indicating more favorable adsorption and greater surface heterogeneity [31]. The Dubinin–Radushkevich model shows higher mean adsorption energy for rGO/ZnO/Fe_2O_3 (4.329 kJ mol^{-1}) than rGO (1.814 kJ mol^{-1}), suggesting stronger interaction strength. The Temkin model also presents higher R^2 for the composite (0.983) relative to rGO (0.964), reflecting differences in adsorbate–adsorbent interaction behavior between the two materials [20, 22, 23].

Table 1. Isothermal adsorption parameters of malachite green on rGO and rGO/ZnO/Fe_2O_3.

Isothermal models	Quantities	rGO	rGO/ZnO/Fe_2O_3
Langmuir	Q_{max} (mg g^{-1})	190.582	305.212
	K_L (L/mg)	0.659-0.162	0.239-0.030
	R_L	0.517	3.180
	R^2	0.985	0.998
Freundlich	n	1.952	2.643
	K_f(mg/g(L/mg)$^{1/n}$)	61.450	199.523
	R^2	0.950	0.930
Dubinin Radushkevitch (D-R)	ε (kJ/mol)	1.814	4.329
	q_D (mg/g)	129.443	246.049
	$B \times 10^{-6}$(mol^2/J^2)	0.152	0.027
	R^2	0.924	0.899
Temkin	b (J/mol)	141.8302	104.4536
	K_T (L/mg)	1.58267 x 10^{-95}	1.43104 x 10^{-30}
	R^2	0.964	0.983

The Dubinin–Radushkevich (D–R) isotherm model provides further insight into the nature of malachite green adsorption on rGO and rGO/ZnO/Fe_2O_3 by estimating the mean adsorption energy (ε), which helps distinguish between physical and chemical interactions. Based on Table 1, the ε value for rGO is 1.814 kJ mol^{-1}, whereas rGO/ZnO/Fe_2O_3 exhibits a higher value of 4.329 kJ mol^{-1}. Since ε values below approximately 8 kJ mol^{-1} are generally associated with physisorption, both systems predominantly involve physical adsorption, however, the higher ε for the composite indicates relatively stronger interaction strength compared to rGO [20,23]. The D–R correlation coefficients (R^2 = 0.924 for rGO and 0.899 for rGO/ZnO/Fe_2O_3) are slightly lower than those obtained from the Langmuir model, suggesting that while the D–R model captures interaction energy trends, monolayer adsorption better represents the equilibrium behavior. The Temkin model further describes adsorbate–adsorbent interactions by considering indirect interaction effects and surface heterogeneity. The Temkin constant b is higher for rGO (141.8302 J mol^{-1}) than for rGO/ZnO/Fe_2O_3 (104.4536 J mol^{-1}), indicating differences in heat of adsorption distribution across the surface. Meanwhile, the Temkin R^2 values remain high (0.964 for rGO and 0.983 for rGO/ZnO/Fe_2O_3), reflecting satisfactory model agreement [31]. When considered alongside the Langmuir and Freundlich parameters, the isothermal analysis reveals that rGO/ZnO/Fe_2O_3 demonstrates higher adsorption capacity and stronger surface interaction characteristics compared to rGO, consistent with the larger Qmax and Kf values observed for the composite system.

Kinetic study of adsorption

The kinetic analysis of malachite green adsorption on rGO shows that the pseudo-second-order model provides a significantly better fit than the pseudo-first-order model across all investigated temperatures, as indicated by the higher correlation coefficients (Table 2). For rGO, the pseudo-first-order R^2 values range from 0.699 to 0.759, whereas the pseudo-second-order model exhibits R^2 values between 0.994 and 0.998, demonstrating much stronger agreement with experimental data. This suggests that the adsorption rate is more accurately described by a model that considers interaction between the adsorbate and active surface sites. The pseudo-second-order rate constant (K_2) for rGO is 0.085 g mg^{-1} min^{-1} at 25°C, slightly decreases to 0.074 g mg^{-1} min^{-1} at 35°C, increases marginally to 0.087 g mg^{-1} min^{-1} at 45°C, and becomes 0.083 g mg^{-1} min^{-1} at 55°C. These variations indicate that temperature influences adsorption kinetics but does not change the dominant kinetic behavior [4]. The consistently higher R^2 values for the pseudo-second-order

model imply that the overall adsorption rate is controlled by surface interaction mechanisms rather than simple diffusion-driven physical adsorption.

Table 2. Comparison of pseudo-first order and pseudo-second order kinetic parameters for rGO and rGO/ZnO/Fe_2O_3.

Adsorbent	Kinetic Model	Parameter	25 ℃	35 ℃	45 ℃	55 ℃
rGO	Pseudo-first order	R^2	0.759	0.723	0.699	0.721
		K_1 (min^{-1})	0.018	0.017	0.015	0.016
	Pseudo-second order	R^2	0.998	0.997	0.996	0.994
		K_2 (g/mg.min)	0.085	0.074	0.087	0.083
rGO/ZnO/Fe_2O_3	Pseudo-first order	R^2	0.809	0.829	0.701	0.876
		K_1 (min^{-1})	0.025	0.027	0.018	0.028
	Pseudo-second order	R^2	0.998	0.998	0.998	0.996
		K_2 (g/mg.min)	0.098	0.092	0.075	0.047

For rGO/ZnO/Fe_2O_3, a similar trend is observed, with the pseudo-second-order model again showing superior fitting performance compared to the pseudo-first-order model. The pseudo-first-order R^2 values range from 0.701 to 0.876, whereas the pseudo-second-order model yields R^2 values of 0.996 to 0.998 across all temperatures. The K_2 values for the composite are 0.098 g mg^{-1} min^{-1} at 25°C, 0.092 g mg^{-1} min^{-1} at 35°C, 0.075 g mg^{-1} min^{-1} at 45°C, and 0.047 g mg^{-1} min^{-1} at 55°C, showing a gradual decrease with increasing temperature. This reduction in rate constant at elevated temperature reflects thermal influence on adsorption dynamics. The higher correlation coefficients for the pseudo-second-order model across both adsorbents indicate that the adsorption process is governed primarily by surface interaction mechanisms involving active site participation rather than solely by mass transfer effects.

Thermodynamic study of malachite green adsorption

The thermodynamic parameters for malachite green adsorption on rGO indicate temperature-dependent behavior, as presented in Table 3. The distribution coefficient (KD) decreases from 2.7736 at 25°C to 1.2075 at 55°C, showing a reduction in adsorption affinity with increasing temperature. The Gibbs free energy (ΔG°) values are negative at all temperatures, ranging from −2.527 kJ mol^{-1} at 25°C to −0.514 kJ mol^{-1} at 55°C, confirming that the adsorption process is spontaneous throughout the investigated range. The progressively less negative ΔG° values at higher temperatures reflect reduced thermodynamic favorability under elevated thermal conditions. The enthalpy change (ΔH°) for rGO is −23.395 kJ mol^{-1}, indicating that the adsorption process is exothermic. The negative entropy change (ΔS°) of −0.070 kJ mol^{-1} K^{-1} suggests decreased randomness at the solid–liquid interface during adsorption, which may be associated with the structured arrangement of dye molecules on the rGO surface. These thermodynamic parameters collectively describe an adsorption process that is spontaneous, exothermic, and accompanied by a reduction in interfacial disorder.

Table 3. Thermodynamic parameters for the adsorption of malachite green onto rGO and rGO/ZnO/Fe_2O_3.

Adsorbent	Temperature	K_D	$\Delta G°$	$\Delta H°$	$\Delta S°$
rGO	25	2.7736	-2.527	-23.395	-0.070
	35	2.2051	-2.025		
	45	1.5000	-1.072		
	55	1.2075	-0.514		
rGO/ZnO/Fe_2O_3	25	32.333	-8.612	-48.720	-0.136
	35	10.236	-5.956		
	45	9.000	-5.809		

	55	4.618	-4.172		

For rGO/ZnO/Fe_2O_3, the thermodynamic parameters show a markedly different magnitude. The K_D values are significantly higher, decreasing from 32.333 at 25°C to 4.618 at 55°C, indicating stronger adsorption affinity compared to rGO. The ΔG° values range from −8.612 kJ mol^{-1} at 25°C to −4.172 kJ mol^{-1} at 55°C, remaining negative across all temperatures and demonstrating spontaneous adsorption. The more negative enthalpy value (ΔH° = −48.720 kJ mol^{-1}) indicates a stronger exothermic character relative to rGO. The entropy change (ΔS° = −0.136 kJ mol^{-1} K^{-1}) is also more negative than that of rGO, reflecting a greater decrease in randomness at the adsorption interface [20, 22]. The magnitude of these parameters reflects stronger adsorbate–surface interactions and a more pronounced thermodynamic driving force in the composite system under the investigated conditions.

Reusability

The reusability performance of rGO/ZnO/Fe_2O_3 was evaluated over ten consecutive adsorption–desorption cycles, as illustrated in Figure 6, to assess structural stability and retention of adsorption efficiency. In the first cycle, the composite achieved a removal efficiency of 97.54%, indicating strong initial adsorption performance. Across subsequent cycles, only minor fluctuations in efficiency were observed, with values ranging from 94.24% to 97.23%. The lowest removal efficiency occurred in the ninth cycle at 94.24%, while the tenth cycle maintained 95.66%, demonstrating that the composite preserved a high proportion of its adsorption capacity after repeated use. The relatively small decrease in performance across cycles suggests that the structural framework of the composite remains largely intact during regeneration. Minor efficiency reduction may be associated with partial blockage of active sites, slight surface fouling by residual dye molecules, or gradual alteration of surface functional groups during repeated adsorption–desorption processes. However, the absence of significant performance deterioration indicates that the incorporation of ZnO and Fe_2O_3 within the rGO matrix contributes to improved structural robustness and resistance to degradation. The stable efficiency profile over ten cycles reflects sustained accessibility of active sites and consistent interaction between the composite surface and malachite green molecules [22, 23]. The limited variation between cycles also implies that the regeneration process effectively restores adsorption capability without inducing substantial morphological or chemical damage. The maintained removal efficiency above 94% throughout all cycles demonstrates repeatable adsorption behavior under the tested conditions and highlights the operational stability of the composite material.

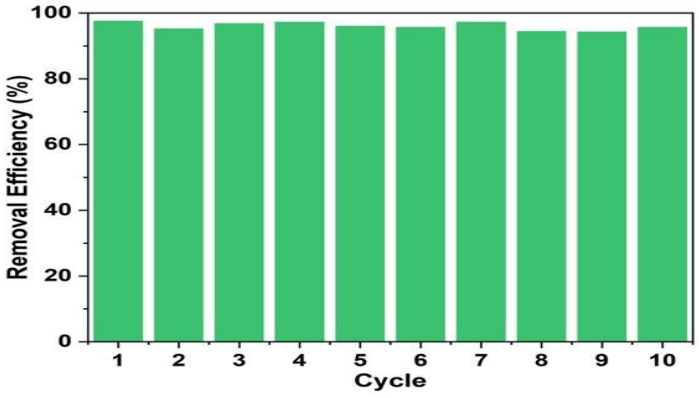

Figure 6. Reusability study of rGO/ZnO/Fe_2O_3 for malachite green removal over 10 cycles.

Mechanism of reduction of graphene oxide

The reduction of graphene oxide (GO) using *Caulerpa peltata* extract is primarily attributed to naturally occurring phytochemicals, particularly polyphenolic compounds, which can act as reducing and stabilizing agents. Polyphenols contain hydroxyl (–OH) groups attached to aromatic structures that can participate in electron- and proton-transfer processes, thereby facilitating the removal or transformation of oxygen-containing functional groups on the GO surface (Figure 7). During the reduction process, phytochemicals in *C. peltata* extract interact with epoxy, hydroxyl, and carboxyl groups present on GO, promoting partial deoxygenation and restoration of the conjugated sp^2 carbon network. The phenolic compounds can undergo oxidation while donating electrons and hydrogen species to oxygenated sites on GO, resulting in a decrease in surface oxygen functionalities. Consequently, the relative proportion of graphitic C=C domains increases, leading to the formation of reduced graphene oxide (rGO). In addition to their reducing activity, biomolecules present in the *C. peltata* extract may adsorb onto the rGO surface and contribute to stabilization by limiting excessive aggregation of the graphene sheets. The structural changes associated with this green reduction process are consistent with the spectroscopic characteristics observed for the synthesized rGO. Overall, *C. peltata* extract provides a bio-derived alternative to conventional chemical reducing agents, enabling the preparation of rGO under comparatively environmentally benign conditions.

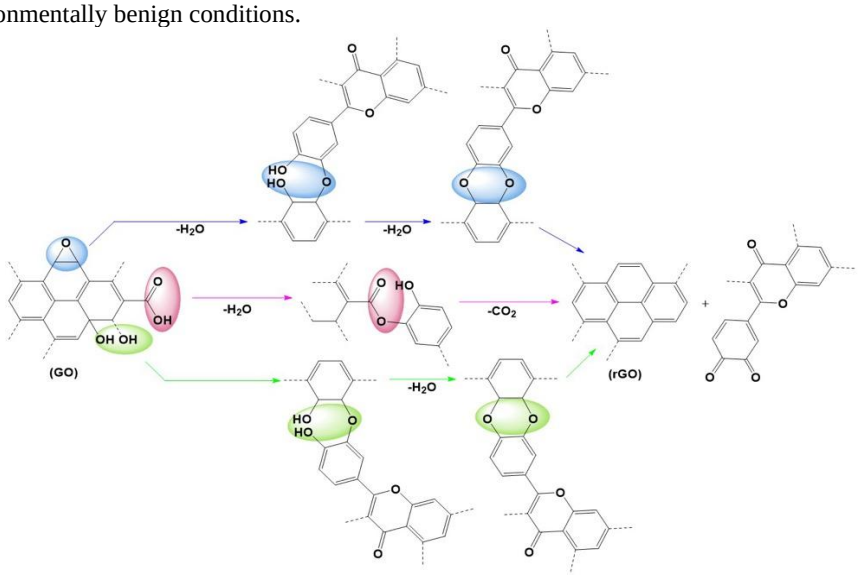

Figure 7. Proposed reduction mechanism of Graphene Oxide

CONCLUSIONS

This study demonstrates the green synthesis of a rGO/ZnO/Fe_2O_3 composite using *Caulerpa peltata* extract as a natural reducing agent and its application for malachite green removal from aqueous solution. The isothermal analysis indicates that rGO/ZnO/Fe_2O_3 exhibits a higher maximum adsorption capacity (305.212 mg g^{-1}) compared to rGO (190.582 mg g^{-1}), reflecting enhanced surface interaction in the composite system. Kinetic modeling shows that the pseudo-second-order model provides the best fit for both materials, with correlation coefficients ranging from 0.996 to 0.998, suggesting that surface interaction mechanisms govern the adsorption rate. Thermodynamic parameters reveal negative $\Delta G°$ values for both adsorbents, confirming

spontaneous adsorption, while negative $\Delta H°$ values (−23.395 kJ mol^{-1} for rGO and −48.720 kJ mol^{-1} for rGO/ZnO/Fe_2O_3) indicate exothermic behavior. The more negative enthalpy value for the composite reflects stronger adsorbate–surface interactions. Reusability testing over ten cycles shows that rGO/ZnO/Fe_2O_3 maintains removal efficiency between 94.24% and 97.54%, demonstrating stable adsorption performance under repeated operation. These findings describe the role of structural integration between metal oxides and graphene sheets in modifying adsorption capacity, kinetic behavior, and thermodynamic characteristics.

ACKNOWLEDGMENTS

We extend our gratitude to the Indonesian Ministry of Research, Technology, and Higher Education for funding this research under contract number 660/UN11.2.1/PG.01.03/SPK/DRTPM/2024, dated June 12, 2024, through the Penelitian Fundamental Reguler (PFR) scheme.

REFERENCES

1. Adeyi, A.A.; Jamil, S.N.A.M.; Abdullah, L.C.; Choong, T.S.Y. Adsorption of malachite green dye from liquid phase using hydrophilic thiourea modified poly(acrylonitrile co acrylic acid). *J. Chem.* **2019**, 2019, 4321475.
2. Ahmad, T.; Manzar, M.S.; Khan, S.U.; Kazi, I.W.; Mu'azu, N.D.; Ullah, N. Synthesis and adsorptive performance of a triazine resin for ultrahigh malachite green removal. *Arab. J. Sci. Eng.* **2023**, 48, 7.
3. Akbar, S.A.; Hasan, M.; Afriani, S.; Nuzlia, C. Phytochemical composition of *Caulerpa taxifolia* and C. peltata. *Biodiversitas* **2023**, 24, 10.
4. Akbar, S.A.; Irham, M.; Hasan, H.A.; Zulfahmi, I.; Iqbal, T.H.; Ahsan, A.; Rahman, M.M.; Jalil, Z. Fluorescent optical sensor for Fe^{3+} detection using *Syzygium aromaticum* derived carbon quantum dots embedded in corn starch biopolymeric film. *Int. J. Biol. Macromol.* **2026**, 359, 151873.
5. Akbar, S.A.; Nuzlia, C.; Hasan, M. Hydrothermally synthesized carbon quantum dots from *Amomum compactum* for fluorescence-based Fe^{3+} sensing. *Malays. J. Fundam. Appl. Sci.* **2026**, 22, 643-653.
6. Arulkumar, A.; Rosemary, T.; Paramasivam, S.; Rajendran, R.B. Phytochemical composition and antioxidant potential of red seaweeds. *Biocatal. Agric. Biotechnol.* **2018**, 15, 1.
7. Bekçi, Z.; Özveri, C.; Seki, Y.; Yurdakoç, K. Sorption of malachite green on chitosan bead. *J. Hazard. Mater.* **2008**, 154, 1-3.
8. Bulut, E.; Özacar, M.; Şengil, I.A. Adsorption of malachite green onto bentonite. *Microporous Mesoporous Mater.* **2008**, 115, 3.
9. de Sá, Í.M.G.L.; Agra, I.M.; Leite, K.J.S.; Oliveira, L.F.A.M.; Fonseca, E.J.S.; Oliveira, L.M.T.M.; Zanta, C.L.P.S.; Duarte, J.L.S. Magnetic MgAl LDH for malachite green removal. *Int. J. Environ. Res.* **2023**, 17, 2.
10. Dou, X.; Zhao, L.; Li, X.; Qin, L.; Han, S.; Kang, S.Z. Ag decorated MoS_2 structure for SERS detection of malachite green. *Appl. Surf. Sci.* **2020**, 5
11. 09, 145331.
12. El-Hout, S.I.; El-Sheikh, S.M.; Gaber, A.; Shawky, A.; Ahmed, A.I. Sunlight photocatalytic degradation over RGO–CuS. *J. Alloys Compd.* **2020**, 849, 156573.
13. Giang, N.T.H.; Hai, N.D.; Thinh, N.T.; Tan, N.N.; Phuong, L.P.; Thinh, D.B.; Van Duc, N.; Viet, V.N.D.; Duy, H.K.; Phong, M.T.; Hieu, N.H. Photocatalytic degradation of malachite green using S doped TiO2/RGO. *Diam. Relat. Mater.* **2022**, 129, 109321.
14. Gunathilaka, T.L.; Samarakoon, K.W.; Ranasinghe, P.; Peiris, L.C.D. Antioxidant and hypoglycemic activity of Gracilaria edulis extract. *Molecules* **2019**, 24, 3708.

15. Gupta, K.; Khatri, O.P. Reduced graphene oxide as adsorbent for malachite green. *J. Colloid Interface Sci.* **2017**, 501, 1.
16. Hulagabali, M.M.; Vesmawala, G.R.; Patil, Y.D. Reduced graphene oxide in cement paste. *J. Build. Eng.* **2023**, 71, 106586.
17. Akbar, S.A.; Hasan, M.; Nuzlia, C. Selective fluorescent detection of ciprofloxacin using carbon quantum dots synthesized from *Amomum compactum*. *Bull. Chem. Soc. Ethiop.* **2026**, 40, 1843-1855.
18. Iqra; Khattak, R.; Begum, B.; Qazi, R.A.; Gul, H.; Khan, M.S.; Khan, S.; Bibi, N.; Han, C.; Rahman, N.U. Green synthesis of silver oxide microparticles for malachite green removal. *Catalysts* **2023**, 13, 227.
19. Khalatbary, M.; Sayadi, M.H.; Hajiani, M.; Nowrouzi, M. γ-Fe2O3/MWCNTs/cellulose for malachite green adsorption. *Biomass Convers. Bioref.* **2024**, 14, 2495-2513.
20. Khoshnamvand, N.; Jafari, A.; Kamarehie, B.; Mohammadi, A.; Faraji, M. Malachite green removal using ZIF-8. *Environ. Process.* **2019**, 6, 3.
21. Mahendran, S.; Maheswari, P.; Sasikala, V.; Rubika, J.J.; Pandiarajan, J. Antioxidant study of red seaweeds. *Toxicol. Rep.* **2021**, 8, 1.
22. Akbar, S.A.; Zulfahmi, I.; Setiawan, I.; Jalil, Z.; Rahman, M.M.; Lahori, A.H. Green synthesis of biomass-derived carbon quantum dots from *Syzygium aromaticum* via carbonization-assisted ultrasonication for a selective colorimetric sensor of Ag^{+} in environmental waters. *Appl. Sci. Eng. Prog.* **2026**, 19, 7925-7925.
23. Palapa, N.R.; Badri, A.F.; Mardiyanto; Mohadi, R.; Taher, T.; Lesbani, A. Mg/Cr LDH for malachite green removal. *Commun. Sci. Technol.* **2022**, 7, 91-97.
24. Parvathi, E.; Akshaya, C.V.; Dilraj, N.; Arjun, G.; Deepak, N.K. Green synthesis of RGO using shallots. *Mater. Today Proc.* **2023**, in press.
25. Piriya, R.S.; Jayabalakrishnan, R.M.; Maheswari, M.; Boomiraj, K.; Oumabady, S. Comparative adsorption of malachite green on acid activated carbon. *Int. J. Environ. Anal. Chem.* **2023**, 103, 16-30.
26. Qaiyum, M.A.; Mohanta, J.; Kumari, R.; Samal, P.P.; Dey, B.; Dey, S. Water chestnut shells as adsorbent for malachite green. *Int. J. Phytoremediation* **2022**, 24, 8.
27. Razaq, A.; Bibi, F.; Zheng, X.; Papadakis, R.; Jafri, S.H.M.; Li, H. Graphene-based flexible composites review. *Mater.* **2022**, 15, 1012.
28. Robati, D.; Rajabi, M.; Moradi, O.; Najafi, F.; Tyagi, I.; Agarwal, S.; Gupta, V.K. Adsorption kinetics of malachite green on GO and RGO. *J. Mol. Liq.* **2016**, 214, 259.
29. Rout, D.R.; Jena, H.M. Malachite green adsorption using RGO/β-cyclodextrin composite. *Int. J. Environ. Anal. Chem.* **2024**, 104, 2.
30. Akbar, S.A.; Jannah, R.; Nuzlia, C.; Hasan, M. Green Valorization of Coconut Husk Waste: NaOH-Activated Carbon for Improved Ammonia Filtration in Recirculating Aquaculture of Common Carp (*Cyprinus carpio*). *Jordan J. Biol. Sci.* **2026**, 19, 113-125.
31. Akbar, S.A.; Satria, E. Uv-Vis study on polyaniline degradation at different pHs and the potential application for acid-base indicator. *Rasayan J. Chem*. **2019**, 12, 1212 - 1218.
32. Akbar, S.A.; Hasan, M.; Jalil, Z.; Zulfahmi, I.; Iqhrammullah, M.; Safina, N. Enhanced ammonia nitrogen filtration using NaOH-activated *Manihot utilissima* peel carbon: Application in recirculating aquaculture systems for Nile tilapia. *Chemosphere* **2025**, 385, 144537.